FEASIBILITY OF NEXT GENERATION NON-LINEAR BEAMFORMING ULTRASOUND METHODS TO CHARACTERIZE AND SIZE KIDNEY STONES

VANDERBILT UNIVERSITY MEDICAL CENTER

RYAN S HSI[1], SIEGFRIED G SCHLUNK[2], JAIME E TIERNEY[2], REBECCA JONES[2], MARK GEORGE[2], PRANAV KARVE[3], RAVINDRA DUDDU[3], BRETT C BYRAM[2]

[1] DEPARTMENT OF UROLOGIC SURGERY, VANDERBILT UNIVERSITY MEDICAL CENTER, [2] DEPARTMENT OF BIOMEDICAL ENGINEERING, VANDERBILT UNIVERSITY, [3] DEPARTMENT OF CIVIL AND ENVIRONMENTAL ENGINEERING, NASHVILLE, TN

INTRODUCTION

- Management of stone disease is primarily dependent on diagnostic imaging to characterize stone burden, location, and associated urinary obstruction.
- Despite advantages of ultrasound over CT, ultrasound suffers from poorer sensitivity, diminished specificity and overestimation of stone size compared to CT.
- There is a need to improve ultrasound-based methods for stones that can overcome the detection and sizing limitations.

- Beamforming methods were applied using a research ultrasound system (Figure 1A).
  - In vivo study for stone contrast and sizing: 5 human stone formers with recent CT <60 days
    - -mean±SD CT stone size 6.0±3.3mm, skin to stone distance 10.2±3.6mm on CT
  - In vitro study for stone shadow: Calcium-based stones (n=12, mean size 8.0 mm, range 2-18mm)
    - -rehydrated and de-gassed at least 24hrs prior to imaging
    - -gelatin phantoms were embedded with graphite to add diffuse scattering.
    - -stones measured at 4 cm and 8 cm depths (Figure 1B).
- Raw channel data were recorded from angled plane wave transmissions ranging between -30° and 30° spaced by 1° using a center frequency of 5.2MHz. The channel data were processed offline in MATLAB (Natick, MA). We assumed a sound speed of 1480 m/sec.
- After the data were processed via the respective algorithms (Ref 1-5) to create each image type (see below table and schematic), the shadow borders were identified using an automated segmentation algorithm implemented in MATLAB (Figure 2, 3).
- Stone contrast (below) and sizing error (= measurement – true size) were compared among the methods.

Figure 1: (A) Verasonics Vantage 128 imaging system. (B) Experimental set-up: water bath with gelatin phantom and kidney stone.

$$contrast_{stone} = 20 * \log_{10} \frac{\mu_{stone}}{\mu_{gel}}$$

where μ is the mean intensity of the stone, shadow, or gelatin background.

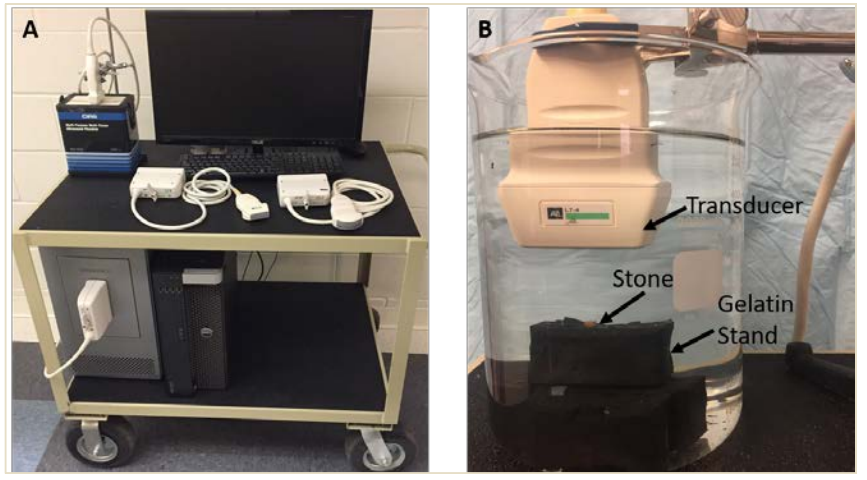

STEPS	B-MODE	PWSF	SLSC	MLSC	ADMIRE
1	Perform transmit beamforming (focus at single depth)	Acquire channel data	Acquire channel data	Acquire channel data	Acquire channel data
2	Acquire channel data	Perform receive beamforming (apply delays)	Perform receive beamforming (apply delays)	Perform receive beamforming (apply delays)	Perform receive beamforming (apply delays)
3	Perform receive beamforming (apply delays)	Perform transmit beamforming (sum plane wave angles)	Perform transmit beamforming (sum plane wave angles)	Compute spatial phase across aperture	Perform transmit beamforming (sum angles)
4	Sum across aperture	Sum across aperture	Compute spatial phase across aperture	Perform transmit beamforming (sum plane wave angles)	Decompose the data into signal of interest and clutter. Sum signal of interest only.

RESULTS

5mm stone in vitro, 8cm depth

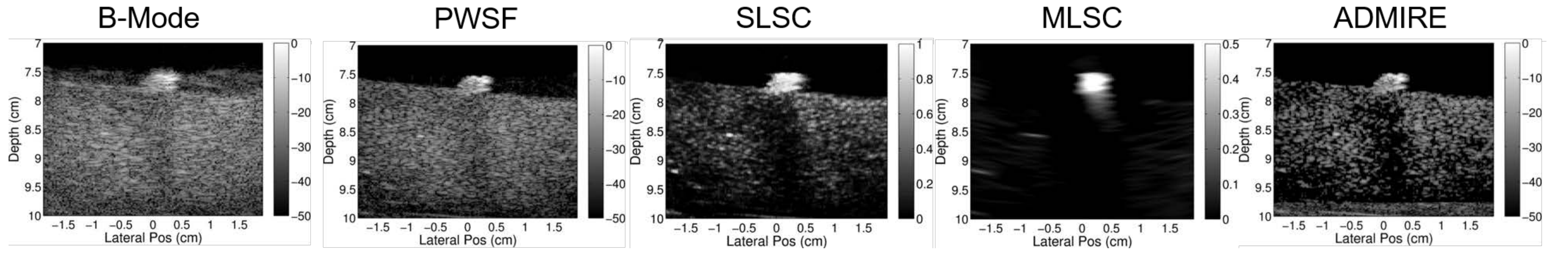

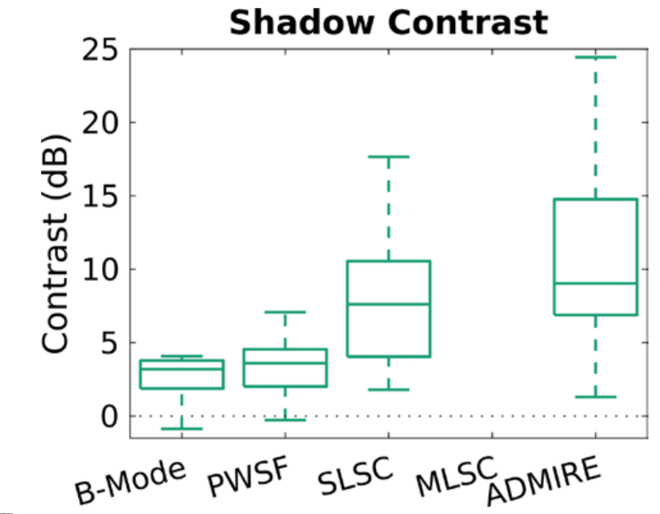

In vitro shadow contrast (dB) comparing the different ultrasound methods. Contrast of the shadow was highest with ADMIRE. With MLSC, a shadow was not visible.

Abbreviations

PWSF - plane wave synthetic focusing
SLSC - short-lag spatial coherence
MLSC - mid-lag spatial coherence
ADMIRE - aperture domain model image reconstruction

Shadow segmentation algorithm

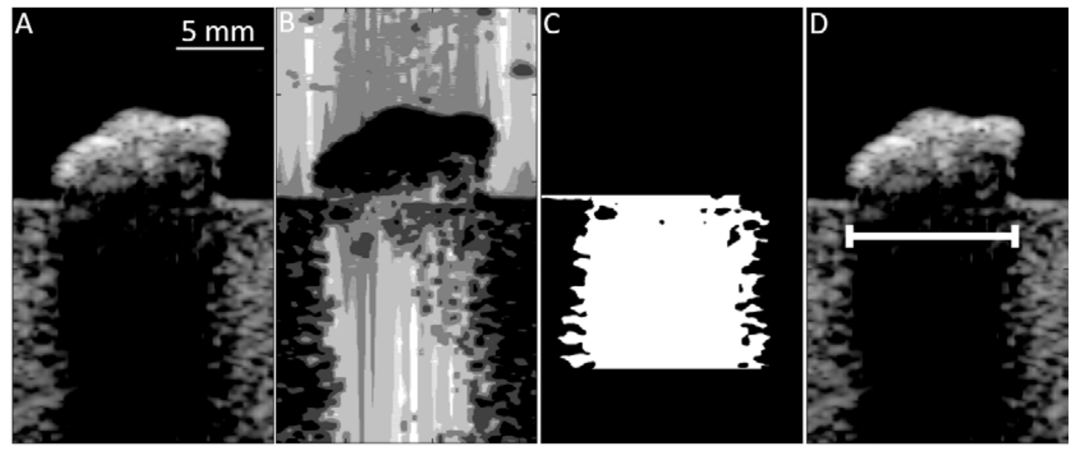

Figure 2: Schematic of automated algorithm to isolate shadow borders based on pixel intensity. A) Original processed image. B) Segmentation algorithm is applied. C) Shadow is selected based on segmentation and depth below stone (up to 1 cm). D) Lateral width is calculated as difference between the average edges of the shadow.

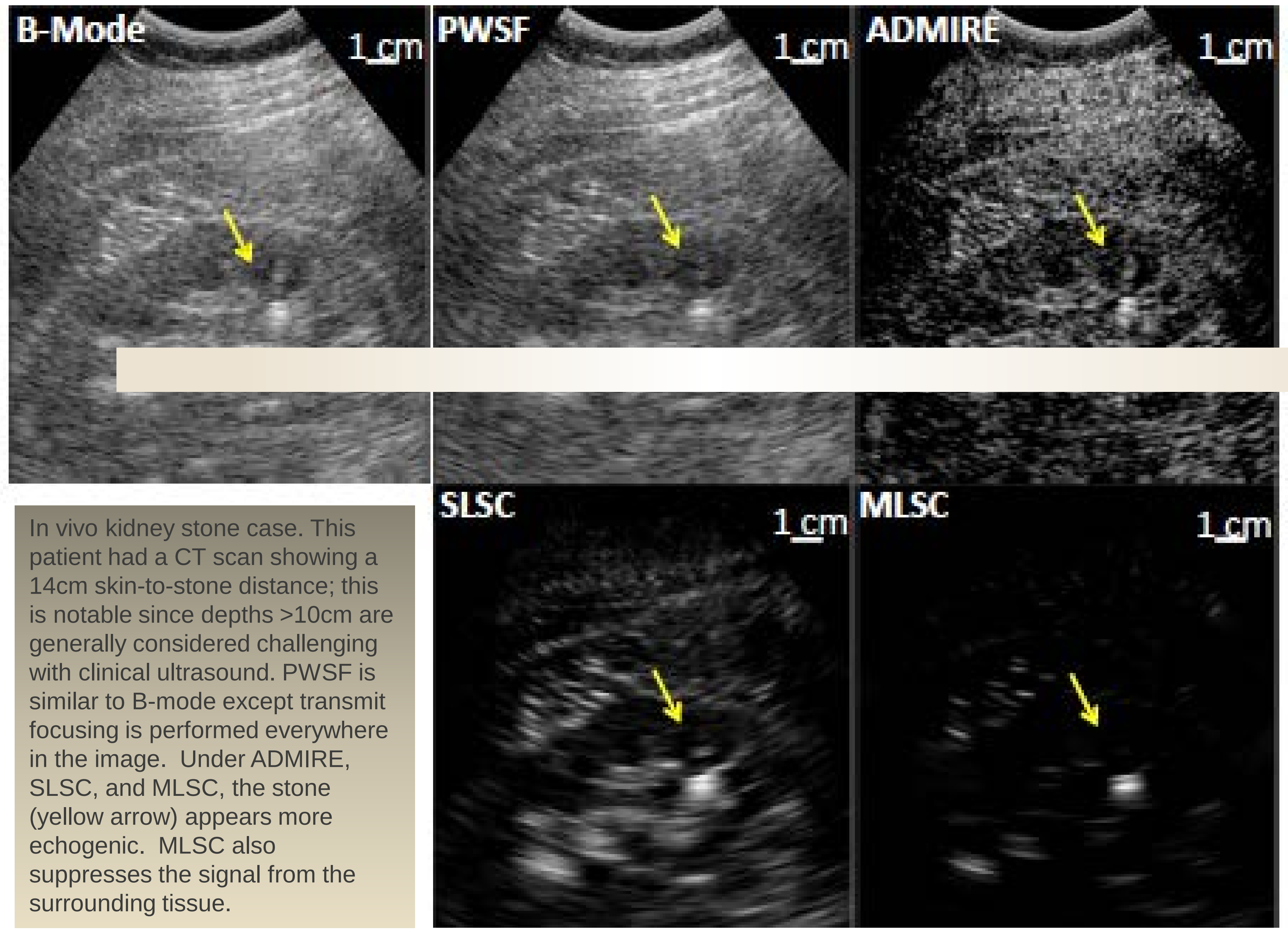

In vivo kidney stone case. This patient had a CT scan showing a 14cm skin-to-stone distance; this is notable since depths >10cm are generally considered challenging with clinical ultrasound. PWSF is similar to B-mode except transmit focusing is performed everywhere in the image. Under ADMIRE, SLSC, and MLSC, the stone (yellow arrow) appears more echogenic. MLSC also suppresses the signal from the surrounding tissue.

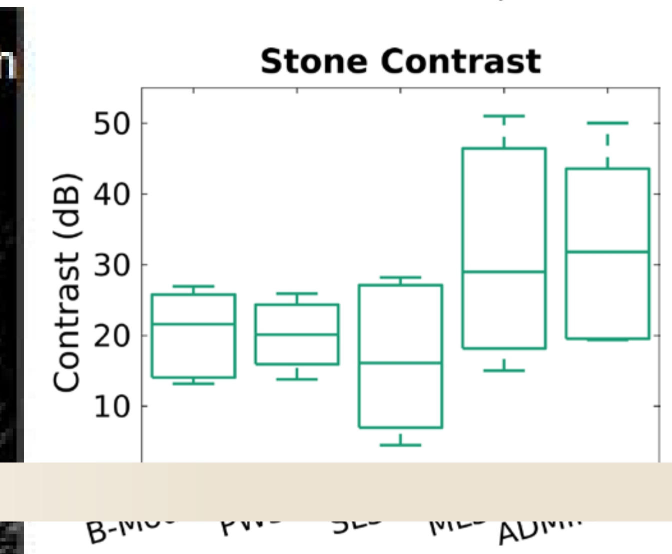

Stone contrast (dB) is best with ADMIRE. SLSC and MLC also show improved SNR and CNR compared to B-mode.

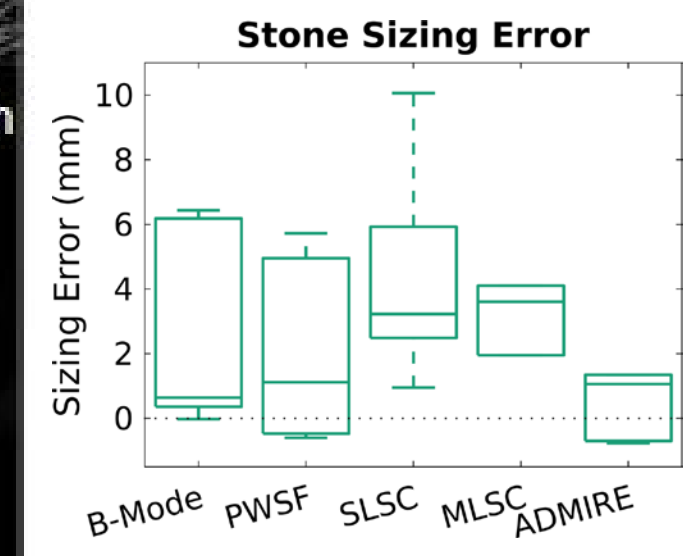

Stone sizing error using CT as the gold standard. ADMIRE had the least mean sizing error (mean +1.3mm error), but when compared to B-mode (mean +2.4mm error), the difference was not statistically significant.

Schematic of generating a single line of an image for each beamforming method.

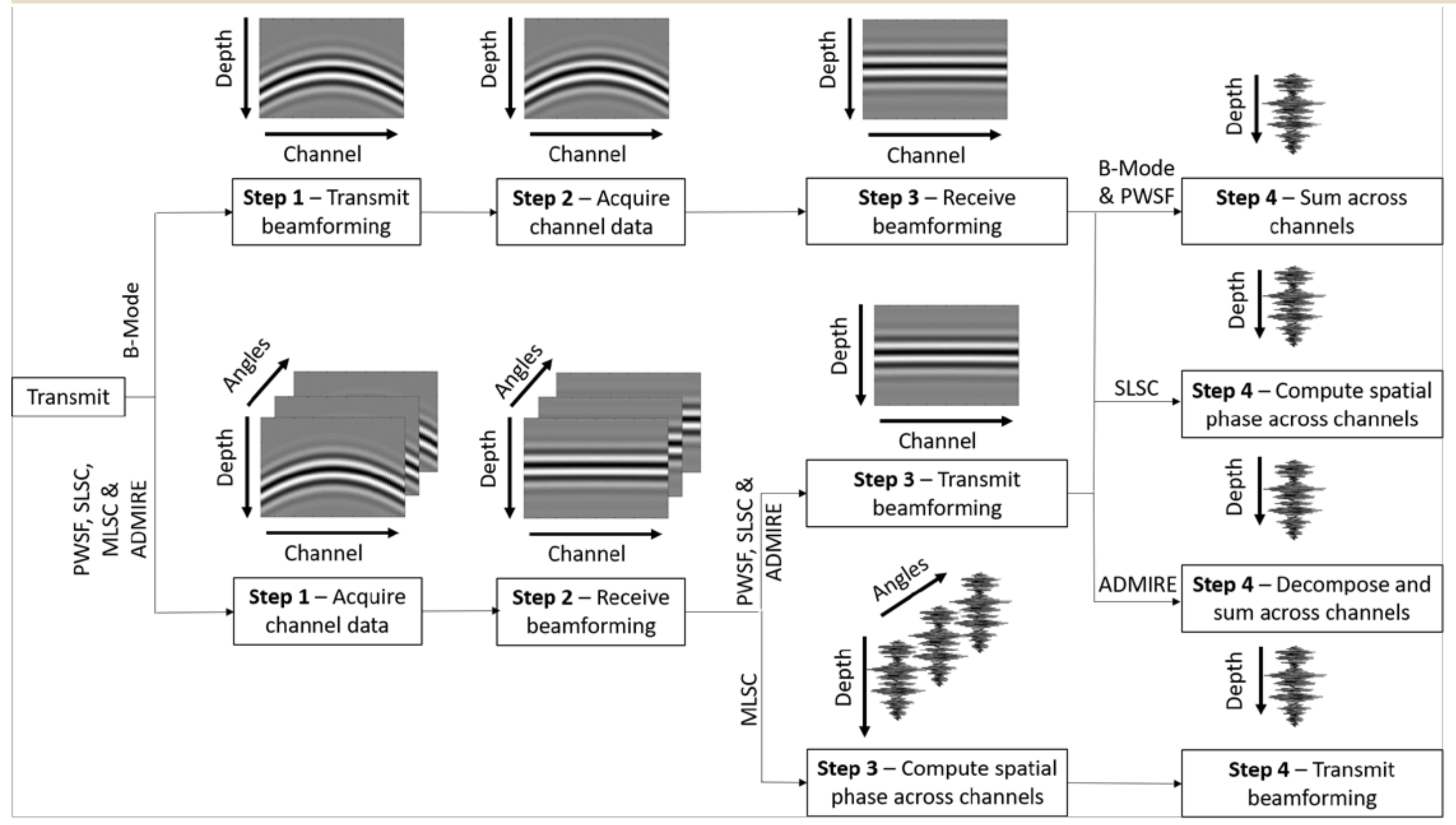

SUMMARY

- Detection and sizing of stones are feasible with advanced ultrasound beamforming methods.
- ADMIRE and MLSC hold promise for improving stone contrast (visibility) over conventional B-mode
- Shadow contrast was best with ADMIRE in vitro.
- Using CT as measurement gold standard, stone sizing error was best with ADMIRE, but did not achieve significance when compared to B mode.

FUTURE WORK

- Image a broader population of human stone formers
- Determine performance characteristics in a blinded study
- Optimize algorithms so they can "backpack" onto existing commercial imaging systems

Acknowledgements

Funding: Vanderbilt Institute of Surgery and Engineering (VISE) Pilot and Feasibility Award, VISE Surgeon in Residence Award, R01EB020040.

References

1. Lediju MA, Trahey GE, Byram BC, Dahl JJ. Short-lag spatial coherence of backscattered echoes: imaging characteristics. IEEE Trans Ultrason Ferroelectr Freq Control. 2011;58:1377-1388.
2. Bottenus N, Byram BC, Dahl JJ, Trahey GE. Synthetic aperture focusing for short-lag spatial coherence imaging. IEEE Trans Ultrason Ferroelectr Freq Control. 2013;60:1816-1826.
3. Byram B, Dei K, Tierney J, Dumont D. A model and regularization scheme for ultrasonic beamforming clutter reduction. IEEE Trans Ultrason Ferroelectr Freq Control. 2015;62:1913-1927.
4. Byram B, Jakovljevic M. Ultrasonic multipath and beamforming clutter reduction: a chirp model approach. IEEE Trans Ultrason Ferroelectr Freq Control. 2014;61:428-440.
5. Montaldo G, Tanter M, Bercoff J, Benech N, Fink M. Coherent plane-wave compounding for very high frame rate ultrasonography and transient elastography. IEEE Trans Ultrason Ferroelectr Freq Control. 2009;56:489-506.
6. Aja-Fernandez S, Curiale AH, Vegas-Sanchez-Ferrero G. A local fuzzy thresholding methodology for multiregion image segmentation. Knowl-Based Syst. 2015;83:1-12.